JGR Solid Earth

RESEARCH ARTICLE
10.1029/2018JB016899

Electrical Investigation of Natural Lawsonite and Application to Subduction Contexts

Anne Pommier[1], Quentin Williams[2], Rob L. Evans[3], Ishita Pal[1], and Zhou Zhang[1]

[1]Institute of Geophysics and Planetary Physics, Scripps Institution of Oceanography, UC San Diego, La Jolla, CA, USA, [2]Department of Earth and Planetary Sciences, UC Santa Cruz, Santa Cruz, CA, USA, [3]Department of Geology and Geophysics, Woods Hole Oceanographic Institution, Woods Hole, MA, USA

Key Points:
- Electrical conductivity of lawsonite is measured up to 10 GPa and 1325 °C
- Electrical transitions at 4.0 and 9.7 GPa are consistent with crystallographic transitions
- Lawsonite dehydration could contribute to high conductivity anomalies in the Cascades

Supporting Information:
- Supporting Information S1
- Table S1
- Table S2

Correspondence to:
A. Pommier,
pommier@ucsd.edu

Citation:
Pommier, A., Williams, Q., Evans, R. L., Pal, I., & Zhang, Z. (2019). Electrical investigation of natural lawsonite and application to subduction contexts. *Journal of Geophysical Research: Solid Earth*, *124*, 1430–1442. https://doi.org/10.1029/2018JB016899

Received 16 OCT 2018
Accepted 27 JAN 2019
Accepted article online 1 FEB 2019
Published online 27 FEB 2019

Abstract We report an experimental investigation of the electrical properties of natural polycrystalline lawsonite from Reed Station, CA. Lawsonite represents a particularly efficient water reservoir in subduction contexts, as it can carry about 12 wt % water and is stable over a wide pressure range. Experiments were performed from 300 to about 1325 °C and under pressure from 1 to 10 GPa using a multi-anvil apparatus. We observe that temperature increases lawsonite conductivity until fluids escape the cell after dehydration occurs. At a fixed temperature of 500 °C, conductivity measurements during compression indicate electrical transitions at about 4.0 and 9.7 GPa that are consistent with crystallographic transitions from orthorhombic C to P and from orthorhombic to monoclinic systems, respectively. Comparison with lawsonite structure studies indicates an insignificant temperature dependence of these crystallographic transitions. We suggest that lawsonite dehydration could contribute to (but not solely explain) high conductivity anomalies observed in the Cascades by releasing aqueous fluid at a depth (~50 km) consistent with the basalt-eclogite transition. In subduction settings where the incoming plate is older and cooler (e.g., Japan), lawsonite remains stable to great depth. In these cooler settings, lawsonite could represent a vehicle for deep water transport and the subsequent triggering of melt that would appear electrically conductive, though it is difficult to uniquely identify the contributions from lawsonite on field electrical profiles in these more deep-seated domains.

1. Introduction

The cycling of volatiles (e.g., hydrogen and carbon) at the planetary scale strongly depends on the capability of subduction zones to carry volatiles to depth and to release some of these volatiles through magmatic processes and arc volcanism. Constraining the volatile budget of the Earth's crust and mantle is the key to understanding the chemistry and physical properties in the planet's interior over time, as the presence of volatiles strongly affects the mineralogical assemblage at depth (e.g., Poli & Schmidt, 2002), lowers the melting point of rocks (e.g., Gaetani & Grove, 1998), impacts the rheological behavior of rocks (e.g., Kohlstedt & Hansen, 2015), and significantly influences the transport properties that govern heat and mass transport (e.g., Chang et al., 2017; Richet et al., 1996; Sifré et al., 2014). In particular, hydrogen is an important volatile element in subduction zones that are locations of significant water flux into the mantle (>10^8 Tg/Myr; van Keken et al., 2011). Among the different water carriers present in subducting slabs, lawsonite ($CaAl_2Si_2O_7(OH)_2{\cdot}H_2O$) represents a particularly efficient reservoir as it can carry about 12 wt % water and is stable to pressures (depths) exceeding those of other hydrous minerals (e.g., talc, antigorite, and chlorite) and to temperatures up to about 800 °C at $P < 5$ GPa (e.g., Pawley, 1994; Poli, 2015; Schmidt, 1995).

Lawsonite is a common mineral in subgreenschist to blueschist facies metamorphic rocks and is also stable at high-pressure and low-temperature conditions, such as for rocks from the ultrahigh pressure eclogite facies (e.g., Tsujimori & Ernst, 2014). In oceanic settings, lawsonite would be found in metamorphosed basaltic crust, and it has been suggested that there is a spatial relationship between lawsonite formation and the presence of serpentinized peridotite in the upper mantle (Vitale Brovarone & Beyssac, 2014). Serpentinite is another primary water carrier into the mantle and is most prevalent where deep faults allow fluids to penetrate through the crust and into the mantle, at slow-spreading ridges (de Martin et al., 2007), at low-angle detachment faults (e.g., Cannat et al., 1995), or where plate bending opens pathways for fluids through the crust (Naif et al., 2015). The relationship between the two minerals, beyond their complementary character as the respective major carriers of water in the oceanic crust and mantle, suggests that settings

Table 1
Starting Composition of Reed Station Lawsonite (wt %)

Oxide	This study[a]	Ransome (1895)
SiO_2	38.42	38.10
Al_2O_3	32.38	28.88
Fe_2O_3	0.81	0.85
CaO	18.37	18.26
MgO	tr	0.23
Na_2O	tr	0.65
TiO_2	tr	-
H_2O	10.02	11.42
Total	*100*	*98.39*

Note. Water content estimated by difference from a total of 100.
[a]From SEM analyses on starting powder. SEM = Secondary Electron Microscope.

with abundant fluid pathways through the crust should similarly transport large fluxes of water into the mantle upon subduction.

Deeper within the subduction system, it has been proposed that lawsonite can be generated from the dehydration of eclogite-facies gabbro (Groppo & Castelli, 2010). The rare occurrence of lawsonite in exhumed HP-LT rocks has been explained by overprint processes during decompression (Vitale Brovarone, 2014). Lawsonite may therefore be a common mineral at depth in subduction, especially in old subducted basaltic crust where temperatures are less high than in young slabs, at metamorphic conditions ranging from low-grade to ultrahigh pressure conditions (e.g., Vitale Brovarone, Alard, et al., 2014), and its physical properties are relevant to the interpretation of geophysical data in subduction zones.

Electrical conductivity, which is sensitive to temperature, pressure, and chemistry, represents a useful and important tool to probe the transport properties of lawsonite and hydrous minerals in general (e.g., Dai et al., 2012; Manthilake et al., 2015; Yoshino et al., 2006). Lawsonite undergoes different crystallographic transitions under pressure (e.g., O'Bannon et al., 2017), and real-time, in situ electrical measurements can also possibly be used to accurately detect phase transformation under pressure. However, electrical studies of lawsonite are scarce. Only one previous experimental study by Manthilake et al. (2015) was conducted on synthetic lawsonite over a wide temperature range at a single pressure (7 GPa), which does not constrain the effect of pressure on lawsonite conductivity. The importance of investigating the electrical response of lawsonite also arises from field electrical (magnetotelluric) studies that observe large conductors in several subduction zones at depths compatible with lawsonite breakdown (≥50-km depth, e.g., Pommier & Evans, 2017). How lawsonite dehydration may contribute to increased conductivity, whether by its presence, its fluid release, and/or through triggering of partial melting, is unclear and requires further work.

Here the results of laboratory experiments at pressures up to 10 GPa and temperatures up to 1325 °C are reported for natural polycrystalline lawsonite. The electrical response of the samples was measured either at fixed pressures over a broad temperature range or at fixed temperatures over a broad pressure range. Phase transitions and dehydration are investigated in the context of previous structural and phase equilibria studies of lawsonite. Based on existing electromagnetic profiles performed in the Cascades and Japan (Hata et al., 2017; McGary et al., 2014), the contribution of lawsonite to field electrical anomalies is also discussed.

2. Experimental Methods

2.1. Starting Material

The starting samples consist of natural lawsonite from the type locality in Reed Station, Tiburon Peninsula, Marin Co., California, USA. The chemical composition of the natural sample is listed in Table 1 and compared with the analysis of Ransome (1895). The major compositional difference with synthetic lawsonite ($CaAl_2Si_2O_7(OH)_2{\cdot}H_2O$) is the presence of minor amounts of Fe and trace amounts of Mg, Na, and Ti. Lawsonite grains were finely crushed (average grain size of ~18 μm) in an agate mortar using acetone and kept in a desiccator until used. This natural composition is representative of lawsonite in subduction zones, and its high-pressure crystallography has been previously characterized up to 10 GPa (O'Bannon et al., 2017).

2.2. Multi-Anvil Electrical Cell Assembly

Electrical experiments were performed in the multi-anvil apparatus in the Planetary and Experimental Petrology Laboratory at University of California San Diego-Scripps Institution of Oceanography using tungsten carbide cubes with a corner-truncation edge length of 8 mm and MgO octahedral pressure media with an edge length of 14 mm (Zhang & Pommier, 2017). Electrical measurements were conducted using the Consortium for Materials Properties Research in Earth Sciences (COMPRES) 14/8 cell assembly adapted for electrical experiments and presented in Figure 1 (Pommier & Leinenweber, 2018).

Sample powder was placed in a high-purity polycrystalline MgO sleeve (ID of 1.5 mm) and surrounded by a rhenium furnace. The sample powder was loaded and directly compacted into the electrical cell. Air was

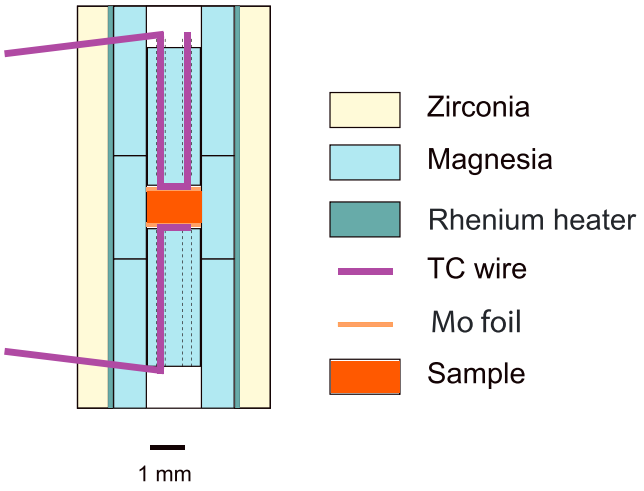

Figure 1. Electrical conductivity cell used in this study (14/8 multianvil COMPRES assembly).

sprayed carefully on the inner wall of the MgO sleeve in order to remove sample powder. The thickness of the sample is about 1.0–1.5 mm. Two molybdenum squares of about 1.5-mm edge length are in direct contact with the lawsonite sample and serve as electrodes. Temperature was monitored using a $W_{95}Re_5$–$W_{74}Re_{26}$ thermocouple, which also acts as one electrode. Another $W_{95}Re_5$ wire was used as a second electrode. All MgO parts were fired at 1400 °C and 1 atm for 1 hr, and then stored in a sealed desiccator until used for the experiments.

2.3. Experimental Protocol

Electrical experiments were conducted on the powdered lawsonite samples over a wide temperature range (300–1325 °C) and up to 10 GPa using a 1,000-t multi-anvil press. Real-time impedance spectra were collected during heating and cooling cycles and during compression and decompression.

Experimental conditions are presented in Table 2. Electrical experiments were conducted either at a defined pressure and varying temperatures or at a fixed temperature (500 °C) over a pressure range. These conditions allow independent exploration of the effect of dehydration and of high-pressure transitions on lawsonite conductivity. In experiments performed at fixed pressure, the cell assembly was first compressed to the target pressure and then temperature was increased. A dwell of more than 12 hr was conducted at 230 °C (i.e., at $T < T_{\text{dehydration}}$) for each experiment to remove absorbed water. These dwell conditions (temperature and duration) are similar to the ones in Manthilake et al. (2015) for synthetic lawsonite samples. Impedance measurements were taken during both heating and cooling cycles at 50 °C intervals at low temperature and at ≤25 °C intervals at high temperature. Measurements were repeated until a stable electrical response was obtained.

In experiments performed at fixed temperature, the sample was compressed to 1 GPa, followed by a 12.5-hr dwell at 230 °C. The sample was then heated to 500 °C and compressed up to 10 GPa, with

Table 2
Experimental Conditions and Electrical Results (Second Heating Cycle)

Sample	Pressure (GPa)	Quenching Temp. (°C)	Dwell duration at 230–250 °C (hr)	Retrieved sample Thickness (mm)	Arrhenius equation parameters				
					T range (°C)	Ln σ_0 (σ_0 in S/m)	Error (S/m)	E_a (kJ/Mol)	Error (kJ/Mol)
Experiments at fixed pressure									
BB157	3.0	975	17	1.55	297–795	4.668	0.029	63.945	0.396
					795–902	28.359	2.042	274.355	19.754
BB104	4.0	1013	17	0.50	246–524	0.900	0.010	38.387	0.422
					524–875	5.420	0.049	68.502	0.623
					875–998	27.032	2.301	275.985	23.569
BB93[a]	4.0	1107	-	1.42	-	-	-	-	-
BB136	5.0	1100	13	0.83	300–677	5.660	0.022	73.024	0.285
					679–930	7.015	0.035	79.892	0.399
BB188	8.0	1325	15	1.30	322–675	2.582	0.018	36.242	0.257
					723–975	0.084	0.013	11.923	1.868
					975–1160	15.963	0.290	178.749	3.253
BB109	9.0	851	13	0.75	400–551	1.753	0.003	20.594	0.037
					551–655	3.643	0.032	33.565	0.299
					655–851	4.690	0.007	41.414	0.066
Experiments at fixed temperature									
BB185	2.0–10	500	12.5	1.40	-	-	-	-	-

[a]Analytical experiment (no electrical measurements).

electrical data being collected every 0.25 GPa or less. Both types of experiments were thermally quenched, by turning off the power to the heater, and subsequently decompressed. The estimated uncertainty on pressure due to heating by 1000 °C under constant load condition is ~0.6 GPa at the peak pressure conditions of 10 GPa and proportionately less at lower pressure and temperature conditions. This estimated error is derived from observed pressure variations on heating in a range of large-volume assemblies (e.g., Leinenweber et al., 2012; Meng et al., 1993), and the small errors result from the observed trade-offs between the competing and compensating effects of thermal pressure (which, for lawsonite and MgO, can be in excess of 3 GPa for 1000 °C of heating at constant volume) and sample relaxation on heating at constant ram load. Thus, these constant ram pressure large volume press experiments lie far closer to constant pressure conditions than the constant volume end-member (Leinenweber et al., 2012). This estimated uncertainty on pressure is possibly smaller than the one associated with phase transformation in lawsonite (transformation causing a change in the sample volume that was accounted for as part of conductivity calculations using the structural study by O'Bannon et al., 2017, as explained below).

2.4. Electrical Measurements and Data Processing

Electrical measurements were performed over the 5 MHz to 10 Hz frequency range using a Solartron 1260 A gain/phase analyzer and the two-electrode technique (e.g., Zhang & Pommier, 2017). Electrical measurements correspond to the recording of the sample's complex impedance (Z) over the frequency range. The real part of the complex impedance corresponds to the electrical resistance R of the sample (e.g., Huebner & Dillenburg, 1995). Electrical conductivity σ was calculated from the measured complex impedance using the relationship

$$\sigma = 1/(R \times G) \tag{1}$$

with R the measured electrical resistance and G the geometric factor (surface area of the electrode/thickness of the sample). The measured resistance corresponds to the response of the sample and the contribution of the electrodes (molybdenum squares, metallic wires, and cables). The latter corresponds to a value of 7.6 Ω over the entire temperature range (Pommier et al., 2015), and this value was subtracted from all resistance values of the samples. The analytical error on electrical conductivity values is determined by accounting for uncertainties on the sample dimensions (diameter and thickness of the sample from the Scanning Electron Microscopy [SEM] images) and the electrical resistance value (Table 2). In the case of Mo square electrodes, this error on conductivity ($\Delta\sigma$) corresponds to

$$\Delta\sigma = |-L/r^2 \times R^2| \times \Delta R + |-2L/R \times r^3| \times \Delta r + |1/R \times r^2| \times \Delta L \tag{2}$$

where l is the sample length, R is the electrical resistance, and r is the length of the side of a square electrode. Values of $\Delta\sigma$ do not exceed a few percent. The change in sample length during compression and dehydration introduces a systematic bias because the final length of the sample usually represents the minimum length for the entire experiment. As pointed out in Pommier and Leinenweber (2018), the final length is reached once the sample reaches the temperature condition where it is soft enough to lose all its porosity (about 800 °C for silicates). Because we cannot estimate these effects well without having an in situ measurement capability, we consider the length after the experiment to be the preferred sample length for conductivity calculations. In the case of the experiment conducted at fixed temperature up to 10 GPa (BB185), the volume change associated with the transitions at 4 and 9.5 GPa and provided in O'Bannon et al. (2017) was accounted for as part of the geometric factor calculations: the sample length was recalculated at each transition, occurring at 4 and 9.7 GPa.

2.5. Analytical Methods

All retrieved samples were mounted in epoxy and polished longitudinally for textural and chemical analyses. Textural analyses were conducted at the UC San Diego SEM Facility in the Nano-Engineering Department. Chemical composition maps and quantitative chemical analyses were performed using Energy-Dispersive Spectrometry (EDS). A 20-kV accelerating voltage was used for the analyses.

3. Results

3.1. Sample Chemistry and Texture

The retrieved experimental samples were not significantly contaminated by the surrounding parts of the electrical cell. Chemical interactions between the sample and the adjacent cell parts (Mo electrodes and MgO sleeve) were characterized using SEM imaging (Figure 2) and EDS analyses. If no contamination of the sample by the electrodes is observed, a thin layer (<80 μm) of orthopyroxene (enstatite) and plagioclase (anorthite) is observed at the MgO sleeve/sample interface in most samples, due to the chemical reaction between MgO and lawsonite during dehydration (Figure 2c). It has been shown that the contribution of a thin layer made of semiconductive material to the bulk conductivity is insignificant (Pommier et al., 2008).

Different minerals were identified in the quenched samples and correspond to breakdown products. As illustrated in Figures 2a and 2b, garnet, zoisite, and kyanite were observed in retrieved samples from experiments at 4 GPa, which is consistent with the breakdown reaction of lawsonite at this pressure (e.g., Manthilake et al., 2015; Pawley, 1994). At 3 GPa, the presence of corundum is observed at the center of the sample (Figure 2c). It is possible that this sample was quenched before complete lawsonite breakdown occurred. An alternative explanation might be that its conditions lie close to (or on) the phase boundary of corundum. Unfortunately, the lawsonite-out curve is not well determined at pressures below 5 GPa (e.g., Pawley, 1994). A thermal gradient across the sample is unlikely to explain the sample's texture as (1) it is <20 °C in these assemblies (Pommier & Leinenweber, 2018), and (2) no chemical gradient has been observed in the other experiments. Experiments at higher pressure (>8 GPa) indicate oxide separation with the presence of small amounts of nonconnected Fe-Ti oxides (Figures 2d).

Using SEM images, we estimate the average grain size in the quenched samples to vary between ~15 and 40 μm (Table 2). These differences can be explained by the variable times spent annealing at low temperature.

3.2. Electrical Results

3.2.1. Impedance Spectra

The electrical response of the samples during frequency scans is characterized in the complex plane, and examples of spectra are presented in Figure 3. The shapes of the spectra strongly depend on temperature, which is in agreement with observations by Manthilake et al. (2015) for synthetic lawsonite. At low temperature ($<T_{\mathrm{dehydration}}$), the samples' response corresponds to a (sometimes slightly flattened) semiarc (Figure 3a) and can be modeled by a resistor in parallel with a constant phase element (e.g., Huebner & Dillenburg, 1995). At high temperature ($>T_{\mathrm{dehydration}}$), the sample's resistance is low and induction effects derived from electrode and W–Re wires control the response at high frequencies (Figure 3b). The electrical resistance is determined as the intersection of the sample response with the real axis. At a fixed temperature of 500 °C under increasing pressure, semiarc spectra were collected up to 10 GPa (Figure 3c).

3.2.2. Effect of Temperature on Lawsonite Conductivity

The electrical conductivity of polycrystalline lawsonite for experiments performed at fixed pressure is presented as a function of temperature in Figure 4a for both heating and cooling cycles. For all samples, electrical conductivity values at a given temperature are similar between the first cooling and the second heating cycles (crosses and filled circles, respectively; Figure 4a), whereas large discrepancies are observed between the first heating and subsequent cycles. These differences between the first heating and the other cycles are consistent with previous electrical studies on synthetic lawsonite (Manthilake et al., 2015) and other silicates, such as olivine (Yoshino et al., 2004; Zhang & Pommier, 2017), and probably reflect thermally activated grain growth processes. The conductivity values discussed below are based on the first cooling and second heating cycles.

For all samples, electrical conductivity strongly increases with temperature and the temperature dependence of lawsonite electrical conductivity can be fit by an Arrhenian formalism over most of the temperature range

$$\sigma = \sigma_0 \times e^{-E_a/(RT)} \tag{3}$$

where σ is the bulk electrical conductivity of the sample (S/m), σ_0 is the preexponential factor (S/m), E_a is the activation enthalpy (J/mol), R is the gas constant, and T is the temperature (K). Values of σ_0 and E_a are listed in Table 2 for all experiments.

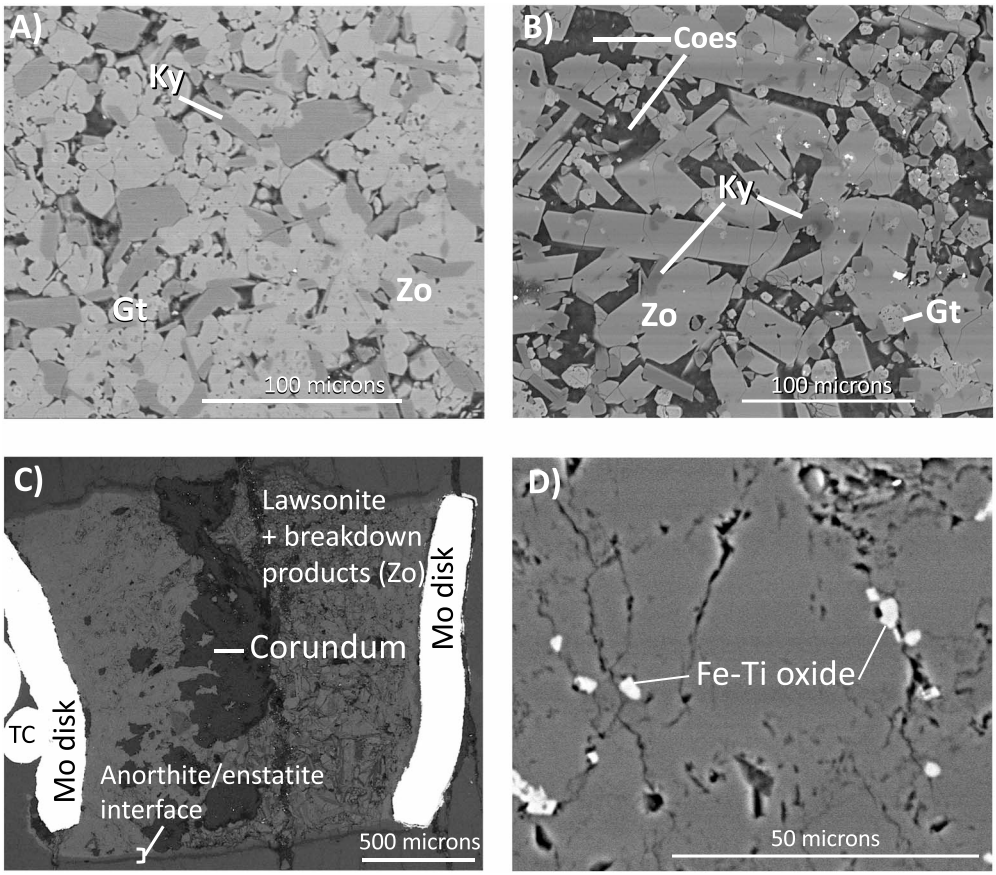

Figure 2. Secondary Electron Microscope (SEM) images of quenched samples. Mineral identification comes from energy-dispersive spectroscopy (EDS) analyses. (a) Retrieved sample from electrical experiment at 4 GPa (BB104). (b) Retrieved sample from analytical experiment at 4 GPa and 1107 °C (BB93), showing different breakdown products (Coes: coesite, Gt: garnet, Zo: zoisite, Ky: kyanite). (c) Retrieved sample from experiments at 3 GPa and 975 °C (BB157). The presence of corundum at the center of the sample corresponds to a major breakdown product at these experimental conditions. The surrounding material corresponds to a mixture of lawsonite and zoisite. Small deformation of the electrode is observed. Electrode deformation is accounted for twice as part of the calculation of uncertainty on conductivity, both through the value of the electrode diameter and of the sample thickness (the two values being part of the calculation of the geometric factor). A thin layer of plagioclase and pyroxene at the sample-MgO sleeve interface results from the interactions between the lawsonite sample and the MgO sleeve during heating. The effect of this layer on the bulk conductivity is negligible (e.g., Pommier et al., 2008, Pommier & Leinenweber, 2018). (d) Presence of Fe-Ti oxides at high pressure (9 GPa, BB109).

Over the investigated temperature range, two or three kinks in slope are observed, characterized either by a smooth or by a sharp change in conductivity. For all samples, a significant conductivity increase occurs between 500 and 700 °C, depending on pressure (Figure 4a). At $T > 800$ °C, a second conductivity increase is observed for all samples and corresponds to a variation in conductivity of more than 1 log unit (Figure 4a). This second transition is followed by a decrease in conductivity at higher temperature.

3.2.3. Effect of Pressure on Lawsonite Conductivity

Electrical results for the experiment performed over the 1–10 GPa pressure range at 500 °C (BB185) are presented in Figure 4b. The effect of pressure on lawsonite conductivity is not insignificant: from 1 to 10 GPa, conductivity varies nonlinearly between 3.3×10^{-4} and 4.2×10^{-2} S/m. This experiment at fixed temperature points out two electrical transitions identified during compression: one transition is observed at about 4.0 GPa and is characterized by a decrease in the effect of pressure on conductivity, while a second transition is identified at about 9.7 GPa by a sharp jump in conductivity (from about 1×10^{-2} to 4×10^{-2} S/m). Accounting for the pressure dependence of E_a in equation (3), the pressure dependence of conductivity corresponds to an activation volume of 2.9 cc/mol for $P < 4$ GPa and negligible ($<10^{-5}$ cc/mol) for

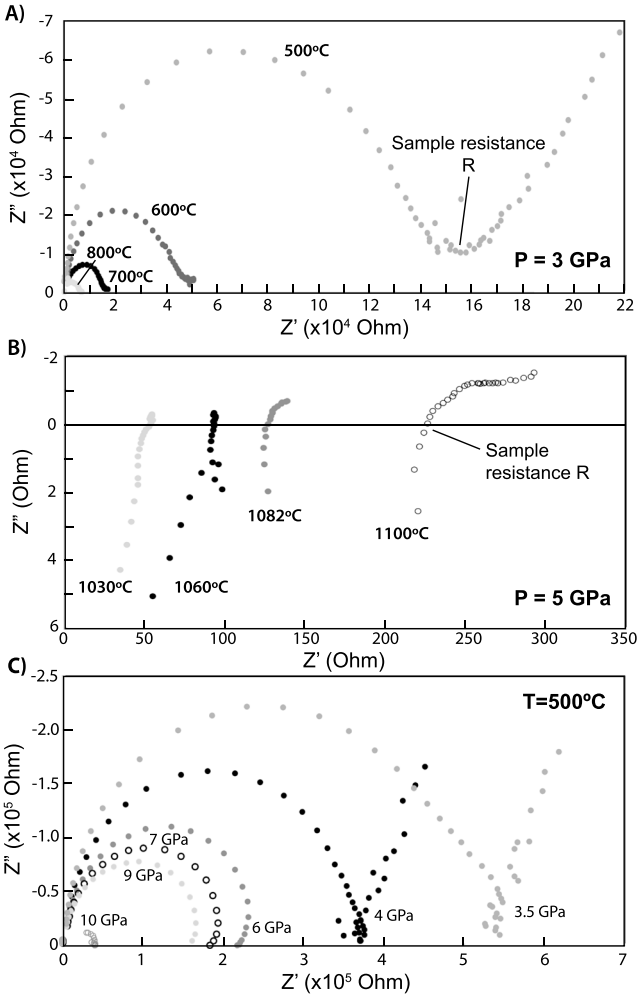

Figure 3. Examples of impedance spectra before (a) and after (b) dehydration of the lawsonite samples at 3 (a, experiment BB157) and 5 GPa (b, experiment BB136), and at 500 °C during compression GPa (c, experiment BB185).

$4 < P < 9$ GPa. The nonlinearity of the pressure effect on conductivity is also noticeable from Figure 4a, where conductivity is comparable between 3 to 5 GPa and increases significantly at 8 and 9 GPa, where it is the highest (at $T < T_{\text{dehydration}}$).

Electrical conductivity values from the experiments at fixed temperature (500 °C) are in broad agreement with the conductivity range of the isobaric experiments (Figure 4a). The small conductivity discrepancies between BB185 and the other experiments are not attributed to sample dehydration, as 500 °C is below the dehydration temperature of lawsonite at these pressures (e.g., Pawley, 1994). A possible explanation may come from the thermal treatment applied to the samples; in the case of experiments at fixed temperature, the initial dwell at 230 °C was performed at 1 GPa, whereas it was performed at the target pressure for experiments at fixed pressures. This may result in differences in the sample's texture and pressure-dependent relaxation processes that can affect the bulk electrical conductivity, though further work is required to understand these mechanisms and their kinetics. The differences in the average grain size between the experiments at fixed temperature and those conducted at 3–5 and 9 GPa are not significant enough to explain the observed difference in conductivity. However, the grain size estimates are for retrieved samples after quench at the highest temperature (i.e., 500 °C for experiments at fixed pressure and >850 °C for experiments at 3–5 and 9 GPa). It is thus not precluded that at 500 °C the average grain size in experiments at 3–5 and 9 GPa was smaller than at T_{quench} and in the experiments conducted at fixed temperature.

4. Discussion

4.1. Electrical Properties of Natural Lawsonite

Most silicate minerals behave as semiconductors at high temperatures. Electrical conduction is controlled by the mobility of lattice defects and of impurities, such as hydrogen (proton conduction) and electron holes hopping between ferrous and ferric iron (small polaron conduction). As pointed out by Yoshino (2010), ionic conduction can be the dominant conduction mechanism at temperatures close to the melting temperature of the mineral and involves the formation of cation vacancies. In the case of hydrous silicate minerals like lawsonite, proton conduction, which consists of charge transfer by proton hopping among point defects, is expected to be the dominant ionic conduction mechanism, in particular at low temperatures due to the low activation energy required for proton conduction (Yoshino, 2010). Polaron hopping is likely to be negligible in our sample, as iron in Reed Station lawsonite is present almost entirely as trivalent iron (Weber et al., 2007).

The electrical conductivity of polycrystalline synthetic lawsonite has been studied at 7 GPa and over a wide temperature range by Manthilake et al. (2015). Comparison between electrical data on the present natural and synthetic lawsonite is illustrated in Figure 5a. A similar dependence on temperature is observed in both studies. The increase in conductivity between 500 and 700 °C may be related to thermally activated defect generation that is directly associated with an incipient phase transition (which is different from defect equilibration within a stable crystal) and mobility within the samples during the first heating cycle. The electrical conductivity of synthetic lawsonite at 7 GPa is close to the conductivity measured on natural lawsonite at 5 GPa, which is in very good agreement with the measured pressure dependence of natural lawsonite conductivity (Figure 4b). A discrepancy in the pressure effect is observed between the two types of lawsonite at high pressure: at 500 °C, a difference in conductivity of about 1 log unit is observed between 7 and 8 GPa (Figure 5a) whereas a difference of a few tenths of a log unit is expected at these conditions (Figure 4b). This difference can be explained by the combined effect of different factors; first, natural lawsonite has

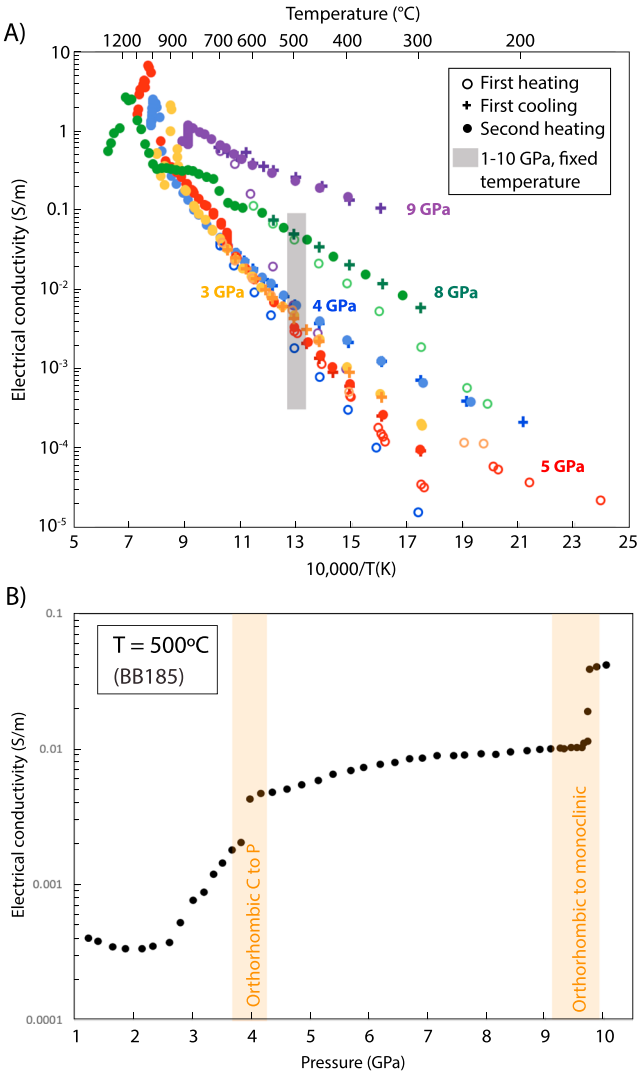

Figure 4. (a) Electrical conductivity results as a function of temperature. The gray area corresponds to the conductivity range obtained at 500 °C over a wide pressure range (BB185). (b) Electrical conductivity results for experiment BB185 conducted at fixed temperature. Color bands indicate the pressure of phase transformations from previous structural studies. See text for details.

small amounts of Fe and Ti (Figure 2d). These elements are not present in the synthetic lawsonite used in Manthilake et al. (2015) and may slow down the mobility of point defects. As electrical conductivity is sensitive to chemistry, the difference in composition likely affects the electrical response of lawsonite. However, the presence of Fe-Ti oxides is unlikely to affect the conductivity dramatically, as they are not present as an interconnected phase. Second, the average grain size in both studies is probably slightly different, resulting from the different amount of time spent at each temperature during the different heating and cooling cycles (despite an initial dwell at 230 °C in both studies). The bigger the grains, the less developed the grain boundary network, and thus the smaller the grain boundary contribution to the bulk conductivity. The higher resistivity of natural lawsonite relative to synthetic lawsonite could also be produced by the average grain size in our experiments possibly being slightly larger than in Manthilake et al. (2015). The sharp decrease in electrical conductivity observed at $T > 800$ °C that follows an increase with increasing temperature (Figure 4a) is consistent with lawsonite dehydration. We interpret the decrease in conductivity as a loss of the aqueous fluid phase from the electrical cell. This decrease was not observed in Manthilake et al. (2015), which may be explained by the fact that in their experiments, temperature was decreased before fluids escaped the cell.

4.2. Electrical Measurements as a Probe of Lawsonite Phase Transitions

As illustrated in Figure 5b, the electrical variations at 500 °C observed at about 4 and 9.7 GPa are consistent with possible crystallographic high-pressure transitions. The sensitivity of electrical conductivity to these transitions makes it a relevant probe of the crystallographic structure of lawsonite at pressure and temperature conditions relevant to subduction contexts. From a technical viewpoint, these findings also highlight the fact that electrical measurements are a relevant technique to calibrate the multi-anvil apparatus in pressure.

The change in electrical conductivity at about 4 GPa occurs at the same pressure as a proposed transition from the orthorhombic C to an orthorhombic P space group at 300 K (Ballaran & Angel, 2003), though this transition has not been systematically observed at this pressure (O'Bannon et al., 2017). If the electrical transition corresponds to this space group change, then the crystallographic transition is accompanied with a decrease in the pressure dependence of lawsonite conductivity (Figure 4b). Comparison with the data from Ballaran and Angel (2003) at room temperature and the electrical data at 500 °C also suggests that this transition does not present a noticeable temperature dependence. Alternatively, the onset of C-forbidden reflections has been observed at pressures above 8 GPa (O'Bannon et al., 2017), and it may be that screw and glide dislocations, which are readily generated in lawsonite (Camara et al., 2001), give rise to forbidden reflections: the presence of such defects could be enhanced at high temperatures. Other possibilities that could give rise to this change in the pressure dependence of conductivity include a shift in the pressure dependence of the dynamic disorder of the protons within the hydroxyl units or water molecules within lawsonite (Libowitzky & Armbruster, 1995; O'Bannon et al., 2017): this parameter is difficult to characterize in either high-pressure diffraction or vibrational studies but could impact proton mobility, and hence electrical conductivity, in this phase.

At about 9.7 GPa, a significant increase in conductivity is observed (Figure 4b). At comparable pressure (9.3 GPa), O'Bannon et al. (2017) observed that the same natural lawsonite undergoes a transition from the orthorhombic to the monoclinic system, which involves a change in the position and hydrogen bonding of H_2O molecules and hydroxyl (OH) groups. Other previous crystallographic studies of lawsonite at room

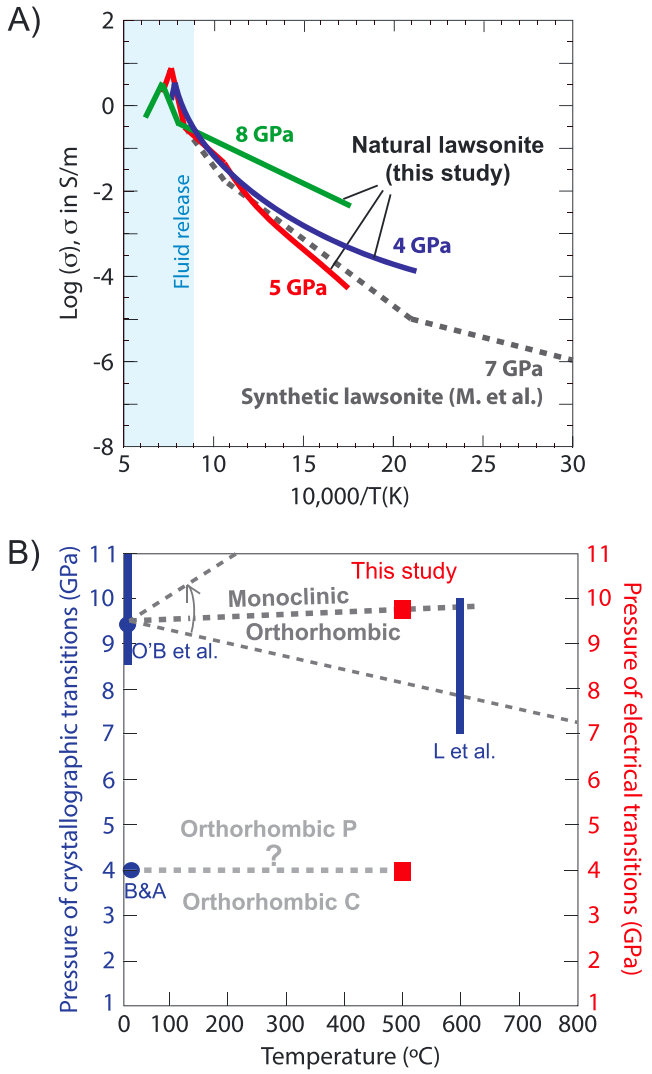

Figure 5. Comparison with previous works on lawsonite. (a) Electrical conductivity of natural (this study) and synthetic (Manthilake et al., 2015) polycrystalline lawsonite. Blue area indicates the breakdown of lawsonite and the release of fluids. (b) Crystallographic transitions from previous studies and electrical transitions at 500 °C. Electrical transitions at 4 and 9.7 GPa are consistent with the orthorhombic P to C and orthorhombic to monoclinic transitions, respectively. O'B et al: O'Bannon et al. (2017 and references therein); B&A: Ballaran and Angel (2003); L et al.: Liebscher et al. (2010).

temperature observed the same transition over a pressure range from 8.6 to 11 GPa (Daniel et al., 2000; Pawley & Allan, 2001), and Liebscher et al. (2010) estimated that at about 600 °C, the transition to the monoclinic structure occurs between 7 and 10 GPa. The addition of the electrical data at 500 °C provides a new constraint on the temperature dependence of the transition (Figure 5b), suggesting a negligible (possibly a very small positive) effect of temperature on the crystallographic change.

Since electrical conduction in solids occurs through the motion of point defects (e.g., Yoshino, 2010), this jump in conductivity underlines that the change in the crystallographic structure facilitates the mobility of charged species. Indeed, the higher conductivity of the high-pressure phase of lawsonite clearly is a result of the high-pressure structure, since the grain size is expected to be constant across the transition due to the close topotactic relation of the low- and high-pressure phases (for example, single crystals are preserved across the transition: Ballaran & Angel, 2003; O'Bannon et al., 2017). The transition is also associated with a larger disorder of the hydroxyl units, and both a decrease in the strength of four of the six Ca-O bonds and a marked increase in the calcium site's distortion (O'Bannon et al., 2017). Hence, both H (derived from hydroxyls) and Ca are likely to be more mobile in the high-pressure phase of lawsonite. The relative roles of the two cations are unclear, but it is notable that the activation enthalpy is the lowest between 400 and 700 °C at 9 GPa (< 34 kJ/mol, Table 2) as the transition is approached (Figure 4a): this lower enthalpy indicates that hydrogen mobility may be important in this pressure/temperature range (e.g., Yoshino, 2010).

4.3. Application to Electromagnetic Studies of Subduction Zones

High-pressure phase transitions in lawsonite are unlikely to be detected by electromagnetic surveys for several reasons. The transition at 4 GPa is characterized by a small variation in conductivity, and the values of conductivity are in ranges that are not well resolved by the magnetotelluric method (Figure 4b). Also, the resolution of the magnetotelluric method degrades with depth and may not be sufficiently sensitive to detect the transition at 9.7 GPa. However, the electrical response of natural lawsonite during dehydration is of interest to the interpretation of electromagnetic profiles performed across subduction zones, as the presence of fluids significantly enhances bulk conductivity (e.g., Pommier, 2014; ten Grotenhuis et al., 2005). The breakdown of lawsonite may be detected by electromagnetic surveys if there is a release of a free aqueous fluid that either forms an interconnected network or triggers partial melting in the mantle wedge (e.g., Pommier & Evans, 2017). However, there are other phases (antigorite for example) that also carry water into the subduction system and breakdown and release water over similar depth ranges (although likely at different locations within the slab), making discriminating the particular source of water release challenging (van Keken et al., 2011).

The stability field and breakdown reactions of lawsonite and other hydrous phases have been studied experimentally over wide pressure and temperature ranges (e.g., Pawley, 1994; Poli, 2015; Schmidt & Poli, 1994). A comparison between phase equilibria experiments, geodynamic models of subduction, and electrical field data is presented in Figure 6. The average *P-T* paths proposed by Penniston-Dorland et al. (2015), using the models from Syracuse et al. (2010) and Gerya et al. (2002), suggest that lawsonite is most likely to breakdown during the subduction of hot young crust. In contrast, lawsonite is mostly stable at the lower temperatures found within older seafloor (e.g., western Pacific), allowing lawsonite to reach significant depths into the mantle.

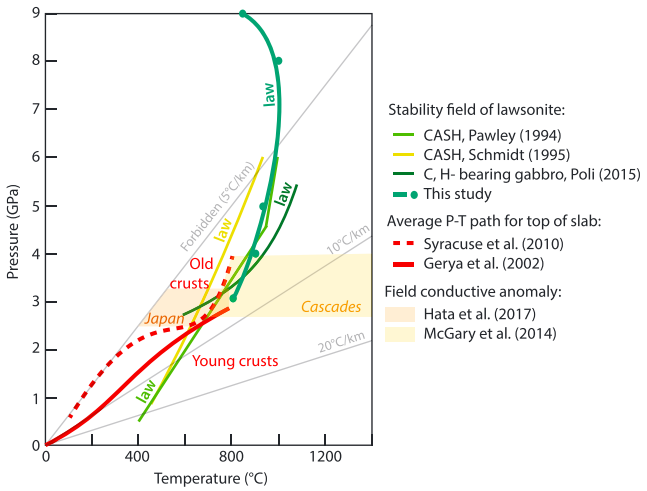

Figure 6. Application to subduction contexts and comparison with electrical field studies. Lawsonite stability field from this and previous studies (Pawley, 1994; Poli, 2015; Schmidt, 1995). CASH: CaO-Al_2O_3-SiO_2-H_2O. Constraints on the stability field from this study (green circles) correspond to the temperature of the base of the conductivity peak observed for each investigated pressure. The best fit to these experimental data (dark green line) is determined visually. Geotherms (gray lines) and average P-T paths of the top of the slab in old/cold subduction zones and young/warm subduction zones are from Penniston-Dorland et al. (2015). Previous studies of lawsonite stability field suggest that lawsonite is stable on most P-T path of old crusts (such as Japan; Hata et al., 2017), and breakdown occurs in young crusts such as Cascadia (McGary et al., 2014) at depths where conductive anomalies are observed (2.5–4 GPa).

The Cascadia subduction system is an end-member example of young subduction (~8 Ma crust) that has been well studied with both magnetotelluric (e.g., Bedrosian & Feucht, 2014; Evans et al., 2014; McGary et al., 2014; Soyer & Unsworth, 2006; Wannamaker et al., 2014) and seismic imaging (Abers et al., 2009; Bostock et al., 2002; McGary et al., 2014; Rondenay et al., 2001, 2008). A common feature for this system is the presence of an electrical conductor at ~50-km depth that is spatially coincident with a change in seismic reflectivity. Even though lawsonite has conductivities in the range of the observed anomalies at the slab temperatures and pressures predicted for Cascadia, it cannot explain by itself the bulk conductivity, as it is a minor phase and is unlikely to form an interconnected network within the crust and/or upper mantle. Instead, the reflectivity has been interpreted as the signal of the basalt-eclogite transition with a release of free aqueous fluids that are thought to be responsible for the conductivity anomaly. Thermal models are consistent with this release of fluid coming from the breakdown of blueschist-lawsonite, and the predicted temperatures within the mantle wedge at the depth of the anomaly are too low for melting to be triggered (van Keken et al., 2011).

Although the fluids released at lawsonite breakdown are conductive, Manthilake et al. (2015) argue, based on the work by Mibe et al. (1999), that fluids released at these low pressures do not form an interconnected network and so would not cause an increase in bulk conductivity to the levels seen in field observations (~0.2 S/m). However, the fact that field electrical (MT) data show large conductive features at depth in agreement with hydrous minerals' breakdown strongly suggests that the fluids are connected (no high conductivity anomaly would be observed if fluids were present as isolated pockets). We assert that, in the laboratory, the fluids released on breakdown likely form an electrical connection through the cell before escaping. As a conservative estimate, if we assume that all of the conduction at the peak is attributed to free fluids in a parallel circuit, then the fluid conductivities range from ~2.5 to 6 S/m over the range of pressure considered.

Sakuma and Ichiki (2016) use molecular dynamics calculations to argue that salinities of 0.5 wt % NaCl are sufficient to explain the conductivity anomalies with fluid fractions of 1%, further pointing out that the critical dihedral angle, and hence connectivity, is a function of fluid fraction. Sakuma and Ichiki (2016) somewhat underestimate the conductivity of the anomaly in the models of McGary et al. (2014) and so likely underestimate either the fluid salinity or volume fraction but not by a large amount: for example, assuming a salinity of 0.5 wt % would require fluid fractions of 3–4 vol %, which is close to the lower bound we calculate from our estimated fluid conductivities. Higher salinities would decrease the amount of fluid required to generate the observed conductivity anomalies. The presence of conductivity anomalies near the locus of dehydration implies that the rate at which fluid migrates away from this region may be slow, and/or that there is a steady state fluid content in this zone. In this context, it is important to note that the region of fluid release/dehydration is likely to be pervasively metasomatized, and the detailed fluid transport characteristics within heavily altered material is likely both heterogeneous and complex (e.g., Zack & John, 2007).

The electrical response beneath the much older (~180 Ma) Pacific plate has been studied in several locations but most notably beneath the Marianas system (Matsuno et al., 2010) and Kyushu Island, Japan (Hata et al., 2017). Beneath Kyushu, Hata et al. (2017) observed a deep conductor contiguous with the top of the slab from a depth of about 70 km down to 100 km (i.e., $\geq \approx$ 2.5 GPa) beneath Unzen and Kirishima volcanoes. The Marianas system features a highly conductive region above the slab starting at depths of about 70 km. In these systems, thermal models suggest that lawsonite would remain stable to great depth (Figure 6). Indeed, temperature estimates from the geodynamic models of the Japan subduction zone by Syracuse et al. (2010) are too low for the breakdown reaction to occur. In this context, the water bonded into lawsonite is expected to be carried down to greater depth, until lawsonite-out reactions occur (these approach pressures of up to about 12 GPa; Schmidt, 1995). In these systems, the signal of lawsonite breakdown, if it

occurs, is likely intermingled with that of other phases leading to a broad region of fluid release. For instance, at the depth of the anomaly beneath Kyushu, chloritoid dehydrates at lower temperature than lawsonite (Schmidt & Poli, 1998), and serpentinite (antigorite) is also expected to contribute to the fluid flux into the system. In these cases, it is simply not possible to geophysically pinpoint the different mineralogic sources of fluid release. Furthermore, at the depths where conductors are seen in these systems, the temperatures can be high enough for melting to be triggered. The high electrical conductivity of volatile-bearing basalts (Ni et al., 2011; Sifré et al., 2014) suggests that a small amount of melt can also reproduce the observed field electrical conductivity values.

5. Concluding Remarks

The electrical conductivity of natural polycrystalline lawsonite was measured at pressure up to 10 GPa and at temperature up to 1325 °C. Two transitions at 4.0 and 9.7 GPa were identified using in situ and real-time electrical measurements; the first may correspond to a transition from orthorhombic C to orthorhombic P symmetry, and the latter is from an orthorhombic to monoclinic transition. At each pressure, lawsonite conductivity increases with temperature (until dehydration occurs). Comparison with field electromagnetic data in subduction settings suggests that lawsonite dehydration could contribute to electrical anomalies observed in the Cascades by releasing aqueous fluid at a depth of about 50 km. In cooler settings such as Japan, lawsonite remains stable at this depth and can therefore carry water to higher depth, where it could potentially contribute to triggering partial melting.

Acknowledgments
A. P. acknowledges financial support from UCSD-SIO startup funds, NSF-EAR Petrology and Geochemistry (grant 1551200), and NSF-COMPRES IV EOID subaward. The use of the COMPRES Cell Assembly Project was also supported by COMPRES under NSF Cooperative Agreement EAR 1661511. Q. W. acknowledges support from NSF EAR-1620423. We thank Kurt Leinenweber for fruitful discussion, Jake Perez for technical help in the lab, and Sabine Faulhaber (UCSD Nano-Engineering Department) for technical assistance with SEM images and EDS analyses. We also thank two reviewers for detailed comments that improved the manuscript. All the electrical data used for Figures 4 and 5 are available in the supporting information.

References

Abers, G. A., MacKenzie, L. S., Rondenay, S., Zhang, Z., Wech, A. G., & Creager, K. C. (2009). Imaging the source region of Cascadia tremor and intermediate-depth earthquakes. *Geology*, *37*, 1119–1122. https://doi.org/10.1130/G30143A.1

Ballaran, T. B., & Angel, R. J. (2003). Equation of state and high-pressure phase transitions in lawsonite. *European Journal of Mineralogy*, *15*(2), 241–246. https://doi.org/10.1127/0935-1221/2003/0015-0241

Bedrosian, P. A., & Feucht, D. W. (2014). Structure and tectonics of the northwestern United States from EarthScope USArray magnetotelluric data. *Earth and Planetary Science Letters*, *402*, 275–289. https://doi.org/10.1016/j.epsl.2013.07.035

Bostock, M. G., Hyndman, R. D., Rondenay, S., & Peacock, S. M. (2002). An inverted continental Moho and serpentinization of the forearc mantle. *Nature*, *417*(6888), 536–538. https://doi.org/10.1038/417536a

Camara, F., Doukhan, J. C., & Carpenter, M. A. (2001). Lattice defects in lawsonite: A TEM investigation. *Mineralogical Magazine*, *65*(01), 33–39. https://doi.org/10.1180/002646101550109

Cannat, M., Mevel, C., Maisa, M., Deplus, C., Durand, C., Gente, P., et al. (1995). Thin crust, ultramafic exposures, and rugged faulting patterns at the Mid-Atlantic Ridge (22–24N). *Geology*, *23*(1), 49–52. https://doi.org/10.1130/0091-7613(1995)023<0049:TCUEAR>2.3.CO;2

Chang, Y., Hsieh, W., Tan, E., & Chen, J. (2017). Hydration-reduced lattice thermal conductivity of olivine in Earth's upper mantle. *Proceedings of the National Academy of Sciences of the United States of America*, *114*, 4078–4081. https://doi.org/10.1073/pnas.1616216114

Dai, L., Li, H., Hu, H., Shan, S., Jiang, J., & Hui, K. (2012). The effect of chemical composition and oxygen fugacity on the electrical conductivity of dry and hydrous garnet at high temperatures and pressures. *Contributions to Mineralogy and Petrology*, *164*, 689–700.

Daniel, I., Fiquet, G., Gillet, P., Schmidt, M. W., & Hanfland, M. (2000). High-pressure behavior of lawsonite: A phase transition at 8.6 GPa. *European Journal of Mineralogy*, *12*(4), 721–733. https://doi.org/10.1127/0935-1221/2000/0012-0721

de Martin, B. A., Sohn, R. A., Canales, J. P., & Humphris, S. E. (2007). Kinematics and geometry of active detachment faulting beneath the Trans-Atlantic Geotraverse (TAG) hydrothermal field on the Mid-Atlantic Ridge. *Geology*, *35*(8), 711–714. https://doi.org/10.1130/G23718A.1

Evans, R. L., Wannamaker, P. E., McGary, R. S., & Elsenbeck, J. (2014). Electrical structure of the central Cascadia subduction zone: The EMSLAB Lincoln Line revisited. *Earth and Planetary Science Letters*, *402*, 265–274. https://doi.org/10.1016/j.epsl.2013.04.021

Gaetani, G. A., & Grove, T. L. (1998). The influence of water on melting of mantle peridotite. *Contributions to Mineralogy and Petrology*, *131*(4), 323–346. https://doi.org/10.1007/s004100050396

Gerya, T. V., Stöckhert, B., & Perchuk, A. L. (2002). Exhumation of high-pressure metamorphic rocks in a subduction channel: A numerical simulation. *Tectonics*, *21*(6), 1056. https://doi.org/10.1029/2002TC001406

Groppo, C., & Castelli, D. (2010). Prograde P-T evolution of a lawsonite eclogite from the Monviso meta-ophiolite (Western Alps): Dehydration and redox reactions during subduction of oceanic FeTi-oxide gabbro. *Journal of Petrology*, *51*(12), 2489–2514. https://doi.org/10.1093/petrology/egq065

Hata, M., Uyeshima, M., Handa, S., Shimoizumi, M., Tanaka, Y., Hashimoto, T., et al. (2017). 3-D electrical resistivity structure based on geomagnetic transfer functions exploring the features of arc magmatism beneath Kyushu, Southwest Japan arc. *Journal of Geophysical Research: Solid Earth*, *122*, 172–190. https://doi.org/10.1002/2016JB013179

Huebner, J. S., & Dillenburg, R. G. (1995). Impedance spectra of hot, dry silicate minerals and rock: Qualitative interpretation of spectra. *American Mineralogist*, *80*(1-2), 46–64. https://doi.org/10.2138/am-1995-1-206

Kohlstedt, D. L., & Hansen, L. N. (2015). Constitutive equations, rheological behavior, and viscosity of rocks. In G. Schubert (Ed.), *Treatise on Geophysics* (Vol. 2, pp. 441–472). Oxford, UK: Elsevier.

Leinenweber, K., Tyburczy, J. A., Sharp, T. G., Soignard, E., Diedrich, T., Petuskey, W. B., et al. (2012). Cell assemblies for reproducible multi-anvil experiments (the COMPRES assemblies). *American Mineralogist*, *97*, 353–368. https://doi.org/10.2138/am.2012.3844

Libowitzky, E., & Armbruster, T. (1995). Low-temperature phase transitions and the role of hydrogen bonds in lawsonite. *American Mineralogist*, *80*(11–12), 1277–1285. https://doi.org/10.2138/am-1995-11-1217

Liebscher, A., Dörsam, G., Franz, G., Wunder, B., & Gottschalk, M. (2010). Crystal chemistry of synthetic lawsonite solid-solution series $CaAl_2[(OH)_2/Si_2O_7]\cdot H_2O$–$SrAl_2[(OH)_2/Si_2O_7]\cdot H_2O$ and the Cmcm–P21/m phase transition. *American Mineralogist*, *95*, 724–735. https://doi.org/10.2138/am.2010.3220

Manthilake, G., Mookherjee, M., Bolfan-Casanova, N., & Andrault, D. (2015). Electrical conductivity of lawsonite and dehydrating fluids at high pressures and temperatures. *Geophysical Research Letters*, *42*, 7398–7405. https://doi.org/10.1002/2015GL064804

Matsuno, T., Seama, N., Evans, R. L., Chave, A. D., Baba, K., White, A., et al. (2010). Mantle electrical resistivity structure beneath the central Mariana subduction system. *Geochemistry, Geophysics, Geosystems*, *11*, Q09003. https://doi.org/10.1029/2010GC003101

McGary, R. S., Evans, R. L., Wannamaker, P. E., Elsenbeck, J., & Rondenay, S. (2014). Pathway from subducting slab to surface for melt and fluids beneath Mount Rainier. *Nature*, *511*, 338–340. https://doi.org/10.1038/nature13493

Meng, Y., Weidner, D. J., Gwanmesia, G. D., et al. (1993). In situ high P-T X-ray diffraction studies on three polymorphs of Mg_2SiO_4. *Journal of Geophysical Research*, *98*(B12), 22,199–22,207. https://doi.org/10.1029/93JB02383

Mibe, K., Fujii, T., & Yasuda, A. (1999). Control of the location of the volcanic front in island arcs by aqueous fluid connectivity in the mantle wedge. *Nature*, *401*(6750), 259–262. https://doi.org/10.1038/45762

Naif, S., Key, K., Constable, S. C., & Evans, R. L. (2015). Water-rich bending faults at the middle America trench. *Geochemistry, Geophysics, Geosystems*, *16*, 2582–2597. https://doi.org/10.1002/2015GC005927

Ni, H., Keppler, H., & Behrens, H. (2011). Electrical conductivity of hydrous basaltic melts: Implications for partial melting in the upper mantle. *Contributions to Mineralogy and Petrology*, *162*(3), 637–650. https://doi.org/10.1007/s00410-011-0617-4

O'Bannon, E. III, Beavers, C. M., Kunz, M., & Williams, Q. (2017). The high-pressure phase of lawsonite: A single crystal study of a key mantle hydrous phase. *Journal of Geophysical Research: Solid Earth*, *122*, 6294–6305. https://doi.org/10.1002/2017JB014344

Pawley, A. R. (1994). The pressure and temperature stability limits of lawsonite: Implications for H_2O recycling in subduction zones. *Contributions to Mineralogy and Petrology*, *118*, 99–108. https://doi.org/10.1007/BF00310614

Pawley, A. R., & Allan, D. R. (2001). A high-pressure structural study of lawsonite using angle-dispersive powder-diffraction methods with synchrotron radiation. *Mineralogical Magazine*, *65*(01), 41–58. https://doi.org/10.1180/002646101550118

Penniston-Dorland, S. C., Kohn, M. J., & Manning, C. E. (2015). The global range of subduction zone thermal structures from exhumed blueschists and eclogites: Rocks are hotter than models. *Earth and Planetary Science Letters*, *428*, 243–254. https://doi.org/10.1016/j.epsl.2015.07.031

Poli, S. (2015). Carbon mobilized at shallow depths in subduction zones by carbonatitic liquids. *Nature Geoscience*, *8*(8), 633–636. https://doi.org/10.1038/ngeo2464

Poli, S., & Schmidt, M. W. (2002). Petrology of subducted slabs. *Annual Review of Earth and Planetary Sciences*, *30*(1), 207–235. https://doi.org/10.1146/annurev.earth.30.091201.140550

Pommier, A. (2014). Geophysical assessment of migration and storage conditions of fluids in subduction zones. *Earth, Planets and Space*, *66*, 38. https://doi.org/10.1186/1880-5981-66-38

Pommier, A., & Evans, R. L. (2017). Constraints on fluids in subduction zones from electromagnetic data. *Geosphere*, *13*, 1036–1041.

Pommier, A., Gaillard, F., Pichavant, M., & Scaillet, B. (2008). Laboratory measurements of electrical conductivities of hydrous and dry Mount Vesuvius melts under pressure. *Journal of Geophysical Research*, *113*, B05205. https://doi.org/10.1029/2007JB005269

Pommier, A., & Leinenweber, K. (2018). Electrical cell assembly for reproducible conductivity experiments in the multi-anvil. *American Mineralogist*, *103*, 1298–1305. https://doi.org/10.2138/am-2018-6448

Pommier, A., Leinenweber, K., & Tasaka, M. (2015). Electrical investigation of the electrical behavior of olivine during partial melting under pressure and application to the lunar mantle. *Earth and Planetary Science Letters*, *425*, 242–255. https://doi.org/10.1016/j.epsl.2015.05.052

Ransome, F. L. (1895). On lawsonite, a new rock-forming mineral from the Tiburon Peninsula, Marin County. University of California, Department of Geological Science Bulletin (Vol. 1, pp. 310–311).

Richet, P., Lejeune, A. M., Holtz, F., & Roux, J. (1996). Rheology of hydrous andesite: An experimental study at high viscosities. *Chemical Geology*, *128*, 185–197. https://doi.org/10.1016/0009-2541(95)00172-7

Rondenay, S., Abers, G. A., & Van Keken, P. E. (2008). Seismic imaging of subduction zone metamorphism. *Geology*, *36*(4), 275–278, https://doi.org/10.1130/G24112A.1

Rondenay, S., Bostock, M. G., & Schragge, J. (2001). Multiparameter two-dimensional inversion of scattered teleseismic body waves. 3. Application to the Cascadia 1993 data set. *Journal of Geophysical Research*, *106*(B12), 30,795–30,807. https://doi.org/10.1029/2000JB000039

Sakuma, H., & Ichiki, M. (2016). Electrical conductivity of NaCl-H_2O fluid in the crust. *Journal of Geophysical Research: Solid Earth*, *121*, 577–594. https://doi.org/10.1002/2015jb012219

Schmidt, M. W. (1995). Lawsonite: Upper pressure stability and formation of higher density hydrous phases. *American Mineralogist*, *80*(11-12), 1286–1292. https://doi.org/10.2138/am-1995-11-1218

Schmidt, M. W., & Poli, S. (1994). The stability of lawsonite and zoisite at high pressures: Experiments in CASH to 92 kbar and implications for the presence of hydrous phases in subducted lithosphere. *Earth and Planetary Science Letters*, *124*(1-4), 105–118. https://doi.org/10.1016/0012-821X(94)00080-8

Schmidt, M. W., & Poli, S. (1998). Experimentally based water budgets for dehydrating slabs and consequences for arc magma generation. *Earth and Planetary Science Letters*, *163*(1-4), 361–379. https://doi.org/10.1016/S0012-821X(98)00142-3

Sifré, D., Gardés, E., Massuyeau, M., Hashim, L., Hier-Majumder, S., & Gaillard, F. (2014). Electrical conductivity during incipient melting in the oceanic low-velocity zone. *Nature*, *509*(7498), 81–85. https://doi.org/10.1038/nature13245

Soyer, W., & Unsworth, M. (2006). Deep electrical structure of the northern Cascadia (British Columbia, Canada) subduction zone: Implications for the distributions of fluids. *Geology*, *34*(1), 53–56. https://doi.org/10.1130/G21951.1

Syracuse, E. M., van Keken, P. E., & Abers, G. E. (2010). The global range of subduction zone thermal models. *Physics of the Earth and Planetary Interiors*, *183*(1-2), 73–90. https://doi.org/10.1016/j.pepi.2010.02.004

ten Grotenhuis, S. M., Drury, M. R., Spiers, C. J., & Peach, C. J. (2005). Melt distribution in olivine rocks based on electrical conductivity measurements. *Journal of Geophysical Research*, *110*, B12201. https://doi.org/10.1029/2004JB003462

Tsujimori, T., & Ernst, W. G. (2014). Lawsonite blueschists and lawsonite eclogites as proxies for paleo-subduction zone processes: A review. *Journal of Metamorphic Geology*, *32*, 437–454. https://doi.org/10.1111/jmg.12057

van Keken, P. E., Hacker, B. R., Syracuse, E. M., & Abers, G. A. (2011). Subduction factory: 4. Depth-dependent flux of H_2O from subducting slabs worldwide. *Journal of Geophysical Research*, *116*, B01401. https://doi.org/10.1029/2010JB007922

Vitale Brovarone, A. (2014). Lawsonite: A delicate, yet fundamental mineral at HP-LT conditions. *Journal of Metamorphic Geology*, *32*, 435–436. https://doi.org/10.1111/jmg.12094

Vitale Brovarone, A., Alard, O., Beyssac, O., Martin, L. A. J., & Picatto, M. (2014). Lawsonite metasomatism and trace element recycling in subduction zones. *Journal of Metamorphic Geology*, *32*, 489–514. https://doi.org/10.1111/jmg.12074

Vitale Brovarone, A., & Beyssac, O. (2014). Lawsonite metasomatism: A new route for water to the deep Earth. *Earth and Planetary Science Letters*, *393*, 275–284. https://doi.org/10.1016/j.epsl.2014.03.001

Wannamaker, P. E., Evans, R. L., Bedrosian, P. A., Unsworth, M. J., Maris, V., & McGary, R. S. (2014). Segmentation of plate coupling, fate of subduction fluids, and modes of arc magmatism in Cascadia, inferred from magnetotelluric resistivity. *Geochemistry, Geophysics, Geosystems*, *15*, 4230–4253. https://doi.org/10.1002/2014GC005509

Weber, S.-U., Grodzicki, M., Geiger, C. A., Lottermoser, W., Tippelt, G., Redhammer, G. J., et al. (2007). ^{57}Fe Mössbauer measurements and electronic structure calculations on natural lawsonites. *Physics and Chemistry of Minerals*, *34*, 1–9. https://doi.org/10.1007/s00269-006-0121-y

Yoshino, T. (2010). Laboratory electrical conductivity measurement of mantle minerals. *Surveys in Geophysics*, *31*(2), 163–206. https://doi.org/10.1007/s10712-009-9084-0

Yoshino, T., Matsuzaki, T., Yamashita, S., & Katsura, T. (2006). Hydrous olivine unable to account for conductivity anomaly at the top of the asthenosphere. *Nature*, *443*(7114), 973–976. https://doi.org/10.1038/nature05223

Yoshino, T., Nishi, M., Matsuzaki, T., Yamazaki, D., & Katsura, T. (2008). Electrical conductivity of majorite garnet and its implications for electrical structure in the mantle transition zone. *Physics of the Earth and Planetary Interiors*, *170*(3-4), 193–200. https://doi.org/10.1016/j.pepi.2008.04.009

Yoshino, T., Walter, M. J., & Katsura, T. (2004). Connectivity of molten Fe alloy in peridotite based on in situ electrical conductivity measurements: Implications for core formation in terrestrial planets. *Earth and Planetary Science Letters*, *222*(2), 625–643. https://doi.org/10.1016/j.epsl.2004.03.010

Zack, T., & John, T. (2007). An evaluation of reactive fluid flow and trace element mobility in subducting slabs. *Chemical Geology*, *239*(3-4), 199–216. https://doi.org/10.1016/j.chemgeo.2006.10.020

Zhang, Z., & Pommier, A. (2017). Electrical investigation of metal-olivine systems and application to the deep interior of Mercury. *Journal of Geophysical Research: Planets*, *122*, 2702–2718. https://doi.org/10.1002/2017JE005390